Appl Water Sci (2017) 7:4301–4319
https://doi.org/10.1007/s13201-017-0573-x

ORIGINAL ARTICLE

Synthesis and characterization of low-cost activated carbon prepared from Malawian baobab fruit shells by H_3PO_4 activation for removal of Cu(II) ions: equilibrium and kinetics studies

Ephraim Vunain[1] · Davie Kenneth[1] · Timothy Biswick[1]

Received: 18 February 2017 / Accepted: 5 May 2017 / Published online: 25 May 2017

Abstract In this study, low-cost activated carbon (AC) prepared from baobab fruit shells by chemical activation using phosphoric acid was evaluated for the removal of Cu(II) ions from aqueous solution. The prepared activated carbon samples were characterized using N_2-adsorption–desorption isotherms, SEM, FTIR, EDX and XRD analysis. The sample activated at 700 °C was chosen as our optimized sample because its physicochemical properties and BET results were similar to those of a commercial sample. The N_2-adsorption–desorption results of the optimized sample revealed a BET surface area of 1089 m^2/g, micropore volume of 0.3764 cm^3/g, total pore volume of 0.4330 cm^3/g and pore size of 1.45 nm. Operational parameters such as pH, initial copper concentration, contact time, adsorbent dosage and temperature were studied in a batch mode. Equilibrium data were obtained by testing the adsorption data using three different isotherm models: Langmuir, Freundlich and Dubinin–Radushkevish (D–R) models. It was found that the adsorption of copper correlated well with the Langmuir isotherm model with a maximum monolayer adsorption capacity of 3.0833 mg/g. The kinetics of the adsorption process was tested through pseudo-first-order and pseudo-second-order models. The pseudo-second-order kinetic model provided the best correlation for the experimental data studied. The adsorption followed chemisorption process. The study provided an effective use of baobab fruit shells as a valuable source of adsorbents for the removal of copper ions from aqueous solution. This study could add economic value to baobab fruit shells in Malawi, reduce disposal problems, and offer an economic source of AC to the AC users.

Keywords Cu(II) ions · Baobab fruit shell · Activated carbon · Adsorption isotherm and kinetics

Introduction

Awareness of water pollution has been a major concern for environmentalists globally. The high level of water contamination is one of the key topics that has attracted attention from research worldwide. The main sources of water contamination include industrialization (chemical industries, e.g. petrochemical, metal plating, paper and pulp, food, leather tanning, pharmaceutical, coal, textile, etc.), municipal wastewater, agricultural activities (use of pesticides and herbicides in agriculture, etc.) and other environmental and global changes (Zhou et al. 2015; Yao et al. 2016a; Trujillo-reyes et al. 2014). Water pollution from heavy metals is a major concern especially in developing countries and Malawi is not an exception. The discharge of effluents containing heavy metals into water resources is a serious pollution problem which affects the quality of water supply. The focus of environmental research has largely been centred on municipal or industrial wastewater because of the potential impact to mankind (Mailler et al. 2016). Municipal and industrial wastewater contains many toxic heavy metals such as chromium (Cr), cadmium (Cd), zinc (Zn), lead (Pb), copper (Cu), iron (Fe), mercury (Hg), arsenic (As), silver (Ag), and the platinum group elements. Discharging these elements into the environment leads to serious soil and water pollution (Nezamzadeh-ejhieh and Kabiri-samani 2013). Increasing

✉ Ephraim Vunain
evunain@cc.ac.mw

[1] Department of Chemistry, Centre for Water and Wastewater Quality, Chancellor College, University of Malawi, P.O.Box 280, Zomba, Malawi

concentrations of these metals in the water poses a serious threat to humans as they are non-degradable and toxic. They can slowly accumulate in the body of human beings thereby exceeding permissible levels, and causing various diseases such as cancer and nervous system damage (Mailler et al. 2016).

Copper is a widely used material especially in the electroplating industry, brass manufacture, mechanical manufacturing industry, copper plumbing, and architecture. Copper waste contamination exists in aqueous waste from copper mining, electronic and electrical industries, industries involved in the manufacture of computer heat sinks, excessive use of Cu-based agro-chemicals, ceramic glazing and glass colouring, etc. Low levels of copper can be found naturally in all water sources. However, when drinking water is allowed to stagnate for a long period of time in household copper pipes, copper levels may rise due to leaching of the pipes. Copper concentrations in drinking water often increase during distribution, more especially in systems with an acidic pH or high-carbonate water with an alkaline pH (WHO 2004). Copper is essential to human health but like all other heavy metals, it is potentially toxic at high concentrations. Furthermore, copper is persistent and bio-accumulative that it does not readily break down in the environment nor is easily metabolized. As a result, it accumulates in the human or ecological food chain through consumption or uptake and may be harmful to both humans and the environment. Copper toxicity may lead to severe mucosal irritation, hepatic and renal damage, capillary damage, central nervous problems followed by depression, gastrointestinal problems in a short term and liver and kidney damage over time (Nebagha et al. 2015). The World Health Organisation (WHO) recommends that the amount of copper in drinking water should not exceed 2.0 mg/L (Nebagha et al. 2015). Public environmental concerns and strict environmental protection have led to global search for novel and low-cost techniques to remove Cu(II) ions as well as other heavy metals from contaminated drinking water and wastewater effluents due to their toxic effects on humans and other forms of life.

A number of treatment technologies are available with varying degree of success to remove Cu(II) ions from aqueous solution. These include among others, ion-exchange, coagulation and flocculation, oxidation–reduction, chemical precipitation, electrochemical methods, adsorption, fixation or concentration (Zhou et al. 2015; Tounsadi et al. 2016). However, most of these treatment processes are costly and in some cases they tend to generate secondary waste by-products. Ultimately, adsorption onto activated carbon (AC) is a well-established and cost-effective technique among the various treatment processes because of its simplicity in design, ease of operation, high adsorption capacity and fast adsorption kinetics used for the removal of heavy metal ions from aqueous solution (Garba and Abdul 2016). Moreover, adsorption processes can remove heavy metal pollutants from aqueous solutions without the generation of hazardous by-products (Zhou et al. 2015). Interesting to note is the fact that activated carbon is widely used for the removal of several pollutants because of its porous structure and surface chemical properties (Rivera-Utrilla et al. 2011; Lu et al. 2012; Luo et al. 2015). Activated carbon is a material that consists of hydrophobic graphite layers and hydrophilic functional groups, high surface area, tuneable pore structure, low acid/base reactivity and thermo-stability, thus making it an effective adsorbent for sorption processes and catalytic applications (Yuen and Hameed 2009; Daud and Houshamnd 2010; Deng et al. 2009; Chen et al. 2012). It has been reported that the surface oxygen-containing functional groups on activated carbon greatly influenced its adsorption performances since the qualities and quantities of these groups affect the adsorption sites, hydrophilicity or hydrophobicity and surface charge distribution on the carbon surface (Scala et al. 2011; Li et al. 2011a, b; Figueiredo et al. 1999; Zhou et al. 2007). In fact, activated carbon has gained global attention as one of the most promising and effective adsorbents for the removal of heavy metal ions from contaminated water and wastewater (Ibrahim et al. 2016; Tounsadi et al. 2016; Lo et al. 2012; Guo et al. 2016; Bohli et al. 2015; Treviño-Cordero et al. 2013; Karnib et al. 2014). The preparation of activated carbon basically involves two stages, namely pyrolysis and activation (physical and chemical activation). However, due to the high production cost, activated carbon tends to be more expensive than other adsorbents and this limits its widespread applications. This limitation has indeed instigated a growing interest in the production of low-cost activated carbons especially from agricultural wastes and other low-cost raw materials (Ghouma et al. 2015; Anisuzzaman et al. 2016; Tounsadi et al. 2016; Mendoza-carrasco et al. 2016; Mailler et al. 2016) that are economically attractive and at the same time show similar or better adsorption performance than commercially available activated carbons. Studies have been reported on the preparation of low-cost ACs for the removal of copper from vegetable waste (Mailler et al. 2016), grape bagasse (Demiral and Güngör 2016), *Elais Guineensis* kernel (Tumin et al. 2008), potato peel (Moreno-Piraján and Giraldo 2011), chestnut shells (Özçimen and Ersoy-Meriçboyu 2009), etc.

Baobab is the common name of the trees of a genus (*Adansonia digitate*), meaning hand-like, in reference to the shape of the leaves. The tree grows in abundance in Malawi and is found to be widely distributed in the southern region of Malawi, lakeshore region in the central

and the northern regions. The baobab tree is very important for humans and animals in the arid regions of Malawi because it can provide shelter, food, clothing and water for the animals and inhabitants of that region (Anchez 2011). Many animals feed on its leaves, flowers and fruits. The fruit, which grows up to a foot long, contains tartaric acid and vitamin C and can either be sucked, or soaked in water to make a refreshing drink. They can also be roasted and ground up to make a coffee-like drink. In Mangochi and surrounding areas, where baobab trees are in abundance, the baobab fruits are collected from the trees and sold to vendors who sell them further to individuals or commercial companies for the production of fruit juice or fruit pulp powder. The fruit shell is a waste produced when the ovoid fruits of the tree are removed from the powdery white flesh seeds. As far as the authors are aware, there is currently no any commercial use for the shells and as such they are often discarded wantonly around the harvesting areas and around the factory's sites, thereby littering the environment.

The aim of the present study is to produce activated carbon from baobab fruit shells by chemical activation using phosphoric acid as a dehydrating agent. The baobab fruit shells as forestry wastes were obtained from Mangochi district of Malawi. To achieve this goal, pyrolysis of the fruit shell, followed by chemical activation was used to obtain abundant, green and environmentally friendly low-cost activated carbon as adsorbent for the removal of Cu(II) ions. The influence of the initial metal concentration, pH, temperature and adsorbent dosage was studied to evaluate the maximum adsorption capacity of the prepared activated carbon as adsorbent. This study was also carried out with the aim of adding value to this category of wastes in Malawi. The results may provide information for estimating the potential of utilizing baobab fruit shell in the production of activated carbon to substitute commercial AC.

Materials and methods

Adsorbate

All chemicals used in this study were of analytical grade. Deionised water was used to prepare solutions of different concentrations. A stock standard copper solution of 1000 mg/L was prepared by dissolving an appropriate quantity of copper in a 1-L volumetric flask and making to the mark with deionised water. The working solutions were prepared by diluting the stock solution with deionized water to give the required concentrations of the working solutions. Six different concentrations of the adsorbate were prepared as 10, 20, 30, 40, 50 and 60 ppm.

Preparation of adsorbent

The baobab fruits were purchased at Mpondabwino Trading Centre in Zomba. Activated carbon was prepared using the chemical activation method according to the procedure by El-Demerdash et al. (2015) with some modifications. Briefly, the baobab fruits were broken to separate the fruit shells from the ovoid seeds (Fig. 1). The fruit shells were then cleaned with distilled water to remove some surface impurities. Thereafter, the shells were broken into pieces of 2–3 cm in size using a mortar and a pestle, and dried in sunlight for 2 days. The pieces were soaked in a solution of 85% phosphoric acid (H_3PO_4) at 1:1.75 (w/w%) impregnation ratio for 24 h at room temperature. After impregnation, the fruit shell samples were air dried at room temperature. Pyrolysis treatment (activation) step was performed as follows: about 100 g of the baobab shell pieces were placed in pre-weighed glass crucibles and carbonized in a muffle furnace for 2.5 h in the absence of oxygen at different temperatures, viz. 200, 300, 400, 500, 600, 700, 800 and 900 °C, respectively. The resulting carbon was ground into powder and washed with 1 L of deionised water to remove residual acid using a Buchner flask and funnel. Finally, the activated carbon was dried at 105 °C for 30 min in an oven and sieved with 106 μm mesh size to obtained fine powder of activated carbon. The powdered activated carbon was kept in air-tight containers and used when required.

Physicochemical characterization of baobab fruit shell-derived activated carbon

Physicochemical properties of the prepared activated carbon were determined according to the standard methods given in the literature (Tounsadi et al. 2016; Brito et al. 2017; Fadhil 2017; Ekpete and Horsfall 2011; Anisuzzaman et al. 2016) and the results are summarized in Table 1.

Determination of carbon yield

The total yield of AC sample was calculated the following equation:

$$\text{Yield } (\%) = \left(\frac{W_t}{W_0}\right) \times 100, \quad (1)$$

where, W_t, is the final mass of the dry impregnated sample at the end of activation process and, W_0, is the initial mass of sample.

Ash content

For the determination of ash content, 1.0 g of the dry AC sample was placed in a porcelain crucible and transferred into a preheated muffle furnace set at a temperature of

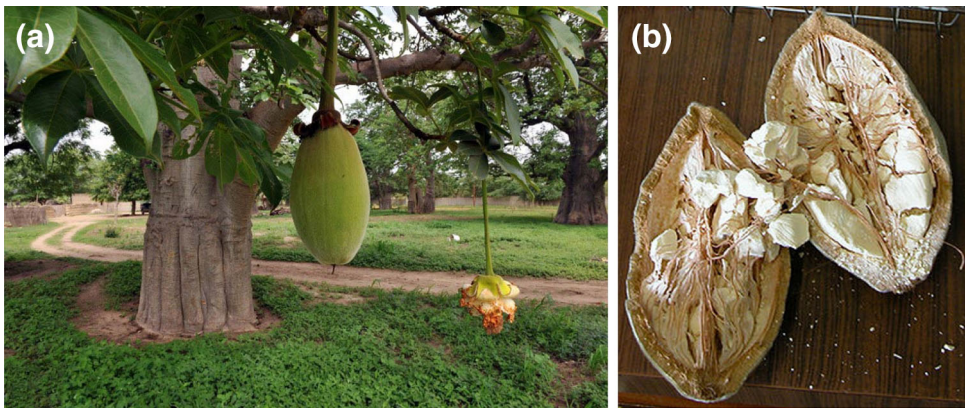

Fig. 1 **a** Baobab tree showing baobab fruit and **b** baobab fruit showing the fruit shells and seeds

Table 1 Carbon yield, ash content, moisture and iodine value of prepared activated carbons

Temperature of carbonization (°C)	Carbon yield (%)	Moisture content (%)	Ash content (%)	Iodine value (mg/g)
200	46	5.78	4.40	550
300	51	3.56	3.39	567
400	55	3.03	2.59	633
500	59	2.98	2.33	658
600	61	2.04	1.84	756
700	78	1.58	1.14	1113
800	78	1.56	1.13	1056
900	80	1.34	1.13	1006

1000 °C. The furnace was left for an hour after which the crucible and its contents were transferred to a desiccator and allowed to cool. After cooling, the crucible and its contents were re-weighed and the weight lost was recorded as the ash content of the AC sample (W_{ash}). Then, the % ash content was calculated using the following equation:

$$\%\ \text{Ash content} = \frac{(W_{\text{ash}}) \times 100}{(W_0)}, \tag{2}$$

where W_{ash} is the weight of the sample after the ash process and W_0 is the dry weight of sample before the ash process.

Moisture content

For the determination of moisture content, 2 g of the AC sample was weighed and dried in a furnace continuously. The drying sample was constantly re-weighed at a 10-min interval until a constant weight (W_{p}) was obtained. The crucible and its content were retrieved and cooled. The difference in weight was recorded and the moisture content (MC) was calculated using the following equation:

$$\text{Moisture content} = \frac{\text{Loss of weight } (2\text{g} - W_{\text{p}})}{\text{Initial dry weight of sample } (W_0)} \times 100 \tag{3}$$

Iodine number

Iodine number often reported in mg/g is a good technique that is often used to determine the adsorption capacity and the quality of activated carbon because of its simplicity and rapid assessment (Tounsadi et al. 2016). It is also a measure of the micropore content of the activated carbon and, therefore, the activity level of the adsorbent. The micropores are responsible for the large surface of AC and are created during activation. Higher levels of iodine number indicate higher degree of activation with typical range between 500 and 1200 mg/g and equivalent to surface area the surface area between 900 and 1100 m^2/g (Tounsadi et al. 2016). In this study, the procedure by Gimba and Musa (2007) was adopted for determination of iodine number. A stock solution was prepared containing 2.7 g of iodine crystals and 4.1 g of potassium iodide per litre. Standardization of the stock solution was done using a standard solution of sodium thiosulphate ($Na_2S_2O_3$). In a typical reaction process, to a 100-mL volumetric flask, 0.5 g of the prepared activated carbon and 10 mL of 5% v/v hydrochloric acid were introduced and the flask was swirled until the carbon was wetted. Then, 100 mL of the stock iodine solution was added and agitated at a fast speed, using a shaker for a period of 60 min. The mixture was filtered through a sintered glass crucible and aliquot portion (20 mL) was titrated with 0.1 M sodium thiosulphate ($Na_2S_2O_3$) using starch as an indicator. The concentration of iodine adsorbed by the AC at room temperature was calculated as the amount of iodine adsorbed in milligrams (Eq. 4).

$$\frac{\text{Img}}{\text{g}} = \frac{(B - S)}{B} \times \frac{VM}{M} \times 253.81, \tag{4}$$

where B and S are the volumes of thiosulphate solution required for blank and sample titrations, respectively. W is the mass of activated carbon sample, M is the concentration (mol) of the iodine solute, 253.81 is the atomic mass of iodine and V is 20-mL aliquot.

Batch equilibrium studies

The effects of solution pH, initial copper concentration, contact time, adsorbent dosage and solution temperature on the uptake of copper onto the AC were investigated. The batch mode was selected because of its simplicity and reliability. Sample solutions were withdrawn at predetermined time interval, filtered through a 0.22-mm pore size membrane and the residual concentration of the copper ion was analysed by atomic adsorption spectrophotometer (AAS). The amount of adsorbate adsorbed at equilibrium, q_e (mg/g) was calculated using Eq. (5) and the percentage removal using Eq. (6).

$$q_e = \frac{(C_0 - C_e)V}{W}, \tag{5}$$

$$\% \text{ Removal} = \frac{(C_0 - C_e)100}{C_0}, \tag{6}$$

where C_0 and C_e (mg/L) are the initial and equilibrium sorbate concentrations, respectively. W is the mass of adsorbent (g) used and V is the volume of the solution (L).

To study the effect of initial copper concentration and contact time on the adsorption uptake, 250 mL of adsorbate solution with known initial copper concentration (10–60 ppm) was prepared in a series of 250-mL conical flasks and 0.2 g AC was added into each flask. The flasks were covered with aluminium foil and placed in an isothermal water bath shaker at constant temperature of 25 °C with rotation speed of 120 rpm for 24 h. For study on effect of adsorption temperature, the experiment was carried out at 25, 30, 35, 40, 45 and 50 °C, respectively. For the effect of solution pH on the copper ions, the adsorption process was studied by varying the solution pH from 3.0 to 12.0. The initial concentration of copper was fixed at 30 ppm with an adsorbent dosage of 0.2 g. Solution temperature and rotation speed of shaker were also fixed at 25 °C and 120 rpm, respectively. The pH was adjusted by adding 0.1 M hydrochloric acid (HCl) and/or 0.1 M sodium hydroxide (NaOH), and was measured using a pH meter. The effect of adsorbent dosage was studied by adding an adsorbent dosage from 0.1 to 1.2 g to a 250-mL solution containing 30 ppm of the metal ions at optimum pH. All other operating parameters were kept constant. To ensure reproducibility and accuracy, each batch adsorption experiments were performed in duplicates and the average values have been reported.

Zeta potential measurements

The zeta potential of the prepared AC was measured using Malvern ZEN 3600 Zetasizer NanoZS instrument equipped with a microprocessor unit. The zeta potential measurements were carried out as a function of equilibrium pH. The suspension pH was adjusted by addition of HCl and NaOH. 0.1-g sample of the prepared AC was weighed into 250-mL conical flasks containing 30 mL of de-ionized water at the desired pH values and shaken for 24 h at 30 °C. The samples were then left to stand for 5 min to allow the particles to settle. Aliquots were taken from the supernatant for zeta potential measurement.

Characterization of adsorbent

Fourier transform infrared (FTIR) spectroscopic analysis was used to study the surface chemistry of both commercial activated carbon and baobab fruit shell-derived activated carbon using a Perkin Elmer Frontier model FTIR spectrometer. A small amount of the dry sample was mixed with KBr powder and the mixture was pressed into pellets, which were then used for analysis. The FTIR spectra were recorded between 4000 and 500 cm^{-1}.

The morphologies of the adsorbents were examined using a JOEL-IT 300 SEM instrument coupled with EDS. Before analysis, the samples were placed on the double-sided carbon conductive tape and were double coated with carbon layer using Quorum Q150R ES instrument to prevent charge accumulation during measurement.

The textural properties of commercial and prepared activated carbon were determined by nitrogen sorption at 77 K after degassing samples at 200 °C for 11 h to ensure dry and solvent-free samples using a Micrometrics ASAP 2020 surface area and porosity analyzer. The relative pressure ratio (P/P_0) was increased from 0 to 1.

The specific surface area (S_{BET}) was calculated according to the Brunauer–Emmett–Teller (BET) method. The total pore volume (V_T) was estimated from the nitrogen adsorbed at a relative pressure of $P/P_0 \sim 0.99$. X-ray diffraction patterns of the baobab fruit shell-derived carbon were obtained using a Rigaku Miniflex Goniometer at 30 kV and 15 mA Cu Kα radiation source ($k = 1.540598$ Å). Samples were scanned over a 2θ range of 5–80° at a scan speed of 0.2 s/step.

Results and discussion

Characterization of adsorbent

Carbon yield, ash content, moisture and iodine number

Important properties such as carbon yield, ash content, moisture content, iodine number of the prepared activated

Table 2 Moisture content, ash content and iodine value characteristics of the commercial AC sample

Moisture content (%)	Ash content (%)	Iodine value (mg/g)
1.08	1.12	1167

carbon which affect the adsorption performance of the adsorbent were determined and the results are presented in Table 1 (baobab fruit shell-derived AC) and Table 2 (for the commercial AC). Carbon yield is the amount of original precursor remaining after pyrolysis and activation treatment. As shown in Table 1, all the eight prepared samples showed a carbon yield within the range of 46–80% as the temperature of carbonization increases. Obviously, one would expect a change in carbon yield under different activation temperatures. The ash content indicates the purity of activated carbon as it measures the amount of residues that remain when the carbonaceous material is burned off. Thus, a low ash content is an indicator of high-purity activated carbon. In this study, a noticeable reduction in ash content was observed at higher temperatures. The reduction in ash content and high carbon yield could be attributed to volatilization of some inorganic constituents at higher activation temperature. It should be noted that activated carbon with low ash content is more preferable for adsorption processes as compared with AC with a high ash content which may interfere with carbon adsorption through competitive adsorption (Nabil et al. 2015; Qureshi et al. 2008). The degree of burn-off increased with increase activated temperatures. These results were consistent with similar results obtained by other researchers (Yusufu et al. 2012; Yang and Lua 2003a; b; Lua et al. 2004). The ash content values of the activated carbon prepared at carbonization temperature of 700, 800 and 900 °C were almost the same with the value obtained for the commercial activated carbon (see Table 1).

The capacity of activated carbon in removing inorganic pollutants from water can also be evaluated through iodine adsorption from aqueous solutions using test conditions referred to as iodine number determination. This indicates their relative activation level and the surface area available for micropores (Akmil-bas and Köseog 2015). Micropores are responsible for the high surface area of ACs and, therefore, adsorption process and are created during activation process. The increase in iodine values as activation temperature increases is a result of development of porosity in the ACs. Usually, higher values within the range of 500–1200 mg/g are a good indicator of a good adsorbent (Tounsadi et al. 2016). Table 1 shows that the iodine values obtained for all the eight prepared samples fall in the range of 550–1113 mg/g. These results also reveal that the AC prepared at 700 °C showed the highest iodine value of

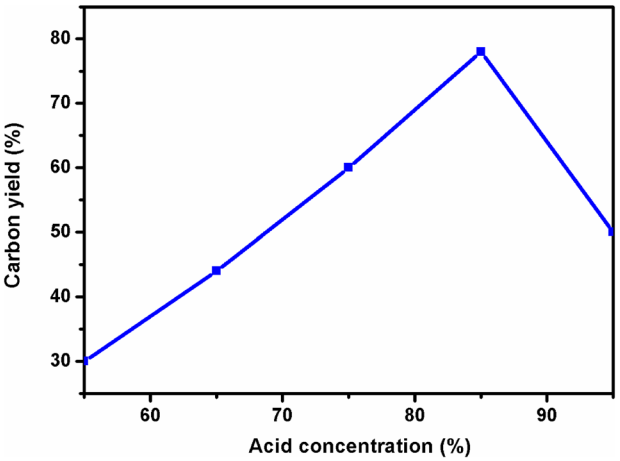

Fig. 2 Effect of acid concentration on the yield of baobab fruit shell-derived AC (optimized sample)

1113 mg/g comparable to the commercial AC sample of 1167 mg/g. The high iodine number demonstrates that baobab fruit shell is an efficient precursor for preparation of carbon with high micropore content. These values are also comparable with those of ACs prepared from other agricultural wastes (Yusufu et al. 2012; Akmil-bas and Köseog 2015). A much higher iodine value obtained for the carbon activated at 700 °C can be attributed to the transformation of amorphous silica to crystalline form that occurred at this temperature. In this study based on the above results, the AC prepared at 700 °C was chosen as our optimized adsorbent for the adsorption process.

Acid concentration

The yield of carbon from a precursor depends largely on the amount of carbon released to bind with oxygen and hydrogen atoms during transformation from lignocellulosic materials (Abimbola et al. 2017). The conversion from lignocellulosic wastes into carbon usually involves the release of O and H atoms in the form of CO_2, CO, H_2O, CH_4 and aldehydes (Tseng 2007). The concentration of the impregnating agent (H_3PO_4) used for the synthesis of the activated carbon was varied from 55 to 95%. Figure 2 illustrates the effect of acid concentration on the yield of baobab fruit shell-derived activated carbon. It is evident from Fig. 1 that the yield (%) of baobab fruit shell-derived AC increased from 30 to 78% as the concentration of H_3PO_4 increased from 55 to 85%, indicating an optimum acid concentration is 85%. Increasing the percentage of H_3PO_4 impregnation increases the release of volatiles on the raw baobab fruit shell, thus an increase in the widening of pore micropores. This mechanism of pore widening had also been reported by other researches (Rodriguez-Reinoso and Molina-Sabio 1992; Ahmadpour and Do DD 1996).

Nitrogen adsorption parameters (BET analysis)

Nitrogen adsorption is one of the standard procedures to determine the porosity of carbonaceous adsorbents, which include surface area, pore size and pore volume. The BET results are shown in Fig. 3 and Table 3. Figure 3 shows that the adsorption–desorption isotherms of optimized AC belongs to the type I isotherm typical of activated carbons as defined by the International Union of Pure and Applied Chemistry (IUPAC) classification. The type I isotherm demonstrates a narrow pore size distribution and relatively small external surface of microporous solids with the limiting uptake being governed by the accessible micropore volume rather than by the internal surface area (Sing et al. 1985). Furthermore, a hysteresis loop is present in the adsorption/desorption isotherms. Hysteresis appearing in the multilayer range of physical adsorption at a relative pressure above 0.3 is usually related to the adsorbent with micropore or mesopore structures. According to the IUPAC nomenclature, porous carbon materials exhibit the H4-type hysteresis loop, which is associated with narrow slit-like pores (Tran et al. 2017) The BET surface areas for the commercial sample and optimized synthesized sample are 1105 and 1089 m^2/g, respectively. The pores formed have sizes smaller than 2 nm, thus indicating the development of microporosity in the synthesized AC. The relatively high surface area of the synthesized optimized sample proved perfect activation at higher temperatures (700 °C). Furthermore, a micropore volume of 0.40 cm^3/g and 0.37 cm^3 for the commercial and the optimized ACs, respectively, were estimated by the *t*-plot method. Similar textural characteristics have been demonstrated by other ACs produced from agricultural wastes (Tounsadi et al. 2016; Lo et al. 2012; Demiral and Güngör 2016; Saka 2012).

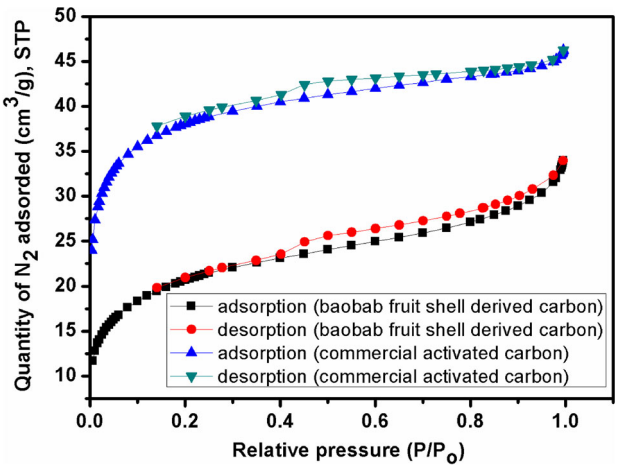

Fig. 3 Adsorption–desorption curves of N_2 at 77 K for commercial AC and baobab fruit shell-derived carbon (optimized sample)

SEM-EDX characterization

Scanning electron microscopy (SEM) technique was used to investigate the surface morphology of the raw baobab fruit shell biomass and optimized activated carbon prepared at 700 °C and results are shown in Fig. 4. The SEM micrographs show a significant difference in the surface morphology of the raw biomass sample without activation and the optimized sample after activation at 700 °C. The surface of baobab fruit shell waste biomass appeared to be covered with thick foreign embodiment with minimum visible porous structures (Fig. 4a, b). Upon H_3PO_4 activation, more porous structures begin to appear which can be attributed to the dehydration effect of H_3PO_4 and the oxidation of organic compounds in the carbonization step (Fig. 4c, d). The SEM images of the activated sample showed an irregular and a well-developed porous structure indicating relatively high surface areas (Fig. 4c, d). After activation, the external surface of the activated carbon has cracks, crevices, and some grains in various sizes in large holes. The availability of pores and internal surface is requisite for an effective adsorbent. With the presence of the large pores, there is a good possibility of the Cu(II) metal ions to be trapped and adsorbed into the pores. Akmil-bas and Köseog (2015) reported a similar observation for the adsorptive properties of orange peel-derived activated carbon. The presence of carbon in the sample is further illustrated by the EDX micrograph in Fig. 5 which shows the presence of C, Mg, Na, Ca and O, and of small amounts of Al, Si, and K. On the basis of these facts, it can be concluded that the prepared activated carbons from baobab fruit shells present an adequate morphology for copper adsorption.

Table 3 Pore structure parameters of the commercial and optimized synthesized AC samples

Sample	Specific surface area (m^2/g)	Pore diameter (nm)	Pore volume (cm^3/g)	
			Micropore volume (cm^3/g)	Total pore volume (cm^3/g)
Commercial AC	1105	1.67	0.4004	0.5008
Synthesized AC (optimized sample)	1089	1.45	0.3764	0.4330

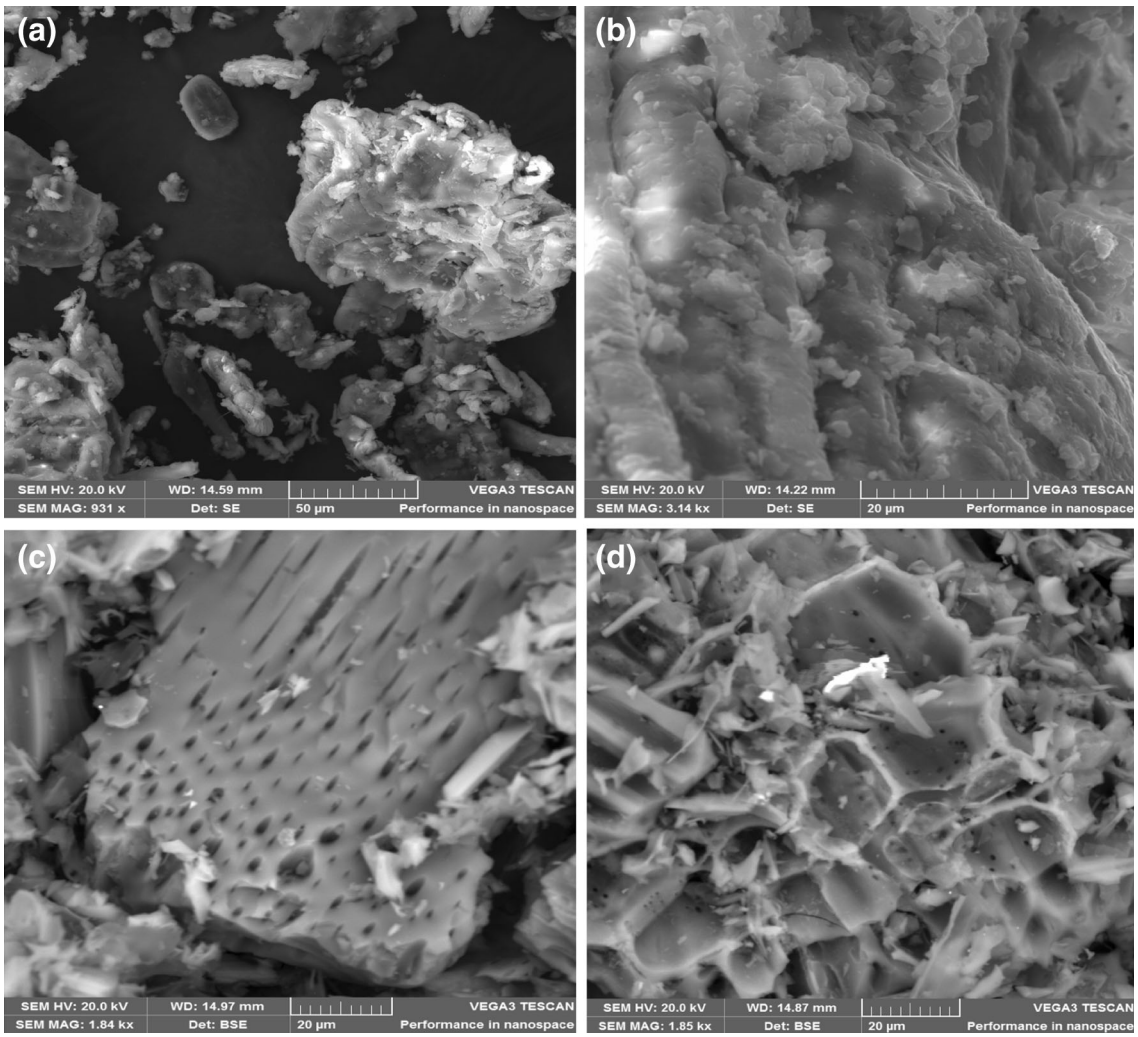

Fig. 4 **a**, **b** Scanning electron microscopy (SEM) micrographs of raw baobab fruit shell biomass; **c**, **d** SEM micrographs of baobab fruit shell-derived activated carbon prepared at 700 °C

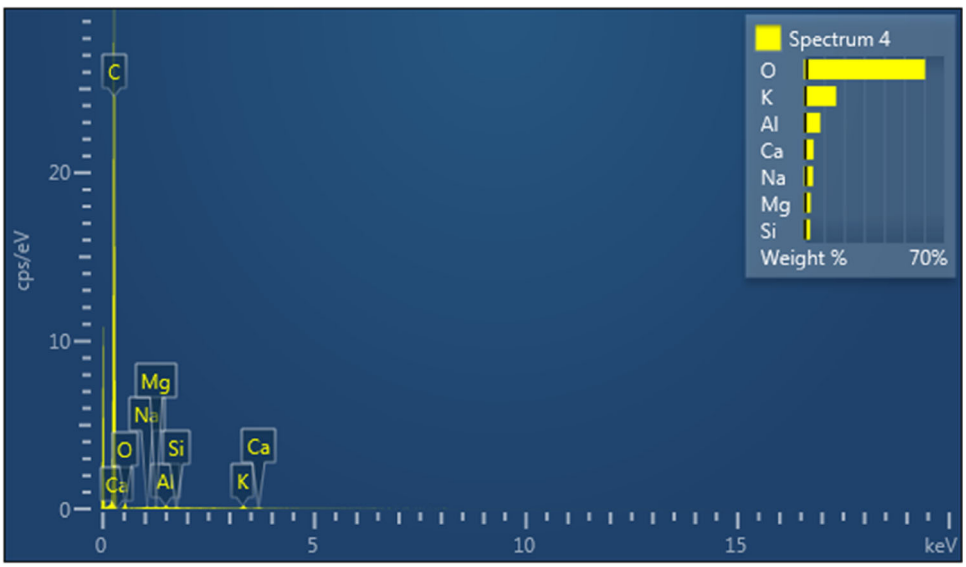

Fig. 5 EDX micrograph of optimized baobab fruit shell-derived carbon (activated at 700 °C) showing the presence of C, Mg, Na, Ca and O, and of small amounts of Al, Si, and K

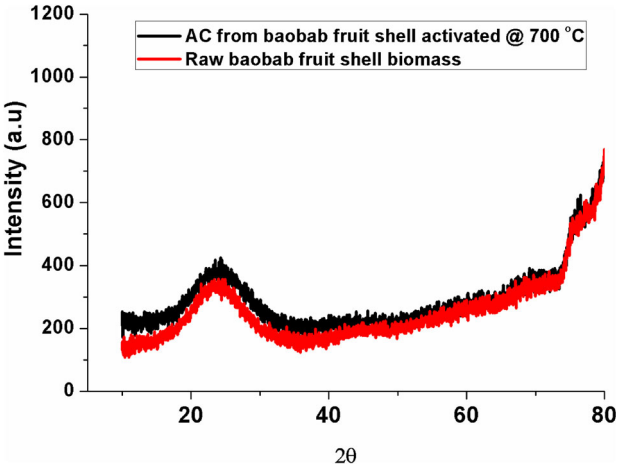

Fig. 6 XRD of raw baobab fruit shell biomass and optimized AC from baobab fruit shell produced at activation temperature of 700 °C

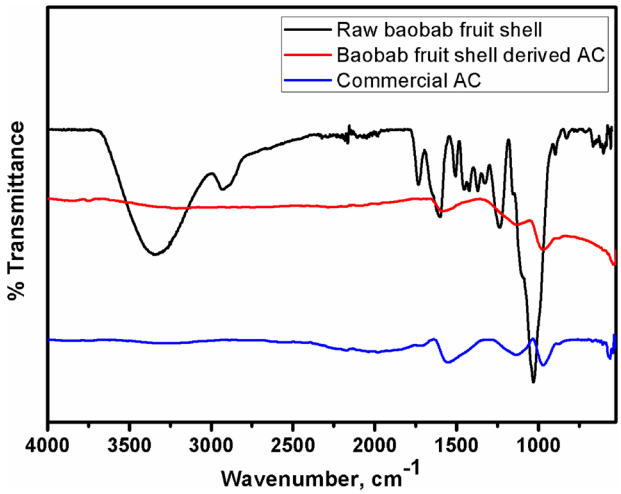

Fig. 7 FT-IR spectra of raw baobab fruit shell biomass, baobab fruit shell-derived activated carbon and commercial AC

X-ray diffraction (XRD) analysis

The prepared activated carbon was also characterized by means of X-ray diffraction. The X-ray patterns of raw baobab fruit shell biomass and activated carbon are shown in Fig. 6. The X-ray diffraction patterns did not exhibit well-defined peaks in any region (defined peaks related to any crystalline phase), which is an indication that no discrete mineral peaks were detected in the samples. Thus, the raw baobab fruit shell biomass and activated carbon had a completely amorphous structure with a noticeable hump in the range 20–30°, which signifies a high degree of disorder, typical of carbonaceous materials. Similar results have been obtained by other researchers working on activated carbon produced from agricultural wastes (Bohli et al. 2015; Köseoglu and Akmil-Başar 2015).

FTIR analysis

The infrared spectra of raw baobab fruit shell biomass, synthesized AC and commercial AC are shown in Fig. 7. As can be observed, the activated carbon spectrum exhibited less absorption bands than raw material spectrum, indicating that some functional groups present in the raw material disappeared after the carbonization and activation steps. This suggests the decomposition of these groups and subsequent release of their by-products as volatile matter by chemical activation at high temperature. The FTIR spectrum of raw baobab fruit shell biomass exhibited absorption bands attributed mainly to hydroxyl and carbonyls groups. For the raw baobab fruit shell biomass, the broad absorption band around 3355 cm^{-1} was ascribed to the presence of hydrogen-bonded O–H groups of cellulose, pectin and lignin. The bands observed at around 2924 and 2853 cm^{-1} were due to C–H symmetric stretching and CH_2 group vibrations. The band around 1655 cm^{-1} is ascribed to the aromatic ring or C=C stretching vibration due to ketones, aldehyde, lactone, and carboxyl (Tongpoothorn et al. 2011). The band at 1500 cm^{-1} is the skeletal C=C vibrations of aromatic rings (Demiral and Güngör 2016). As baobab fruit shell biomass is activated with H_3PO_4, the sharp absorption band between 900 and 1200 cm^{-1} may be attributed to the presence of phosphorus species in the samples (Liou 2010). Meanwhile, the synthesized and commercial ACs present a similar profile with different intensities. The weak bands in the range 1550–1450 cm^{-1} are due to the C=C stretching that can be attributed to the presence of benzene rings or aromatic rings. The weak bands in the range of 1300–900 cm^{-1} are usually assigned to the C–O stretching vibration in acids, alcohols, phenols, esters and/or esters groups, aromatic rings (Akmil-bas and Köseog 2015) and C–H bending, respectively.

Batch equilibrium studies

Effect of pH and zeta potential

Hydrogen ion concentration in the adsorption processes is considered to be one of the most important parameters that could influence the behaviour of Cu(II) in aqueous solutions. Hydrogen ion concentration affects the solubility of heavy metal ions in the solution. It also affects the degree of ionization of the adsorbate during reaction and replaces some of the positive ions that could be found in the active sites of the adsorbent (Kilic et al. 2011). The effect of solution pH was studied between pH 3.0 and 12.0 with 30 ppm Cu(II) at 25 °C and the results are shown in Fig. 8. The uptake of copper increases from 2.52 to 3.13 mg/g when the pH increases from 3.0 to 6. The results indicate

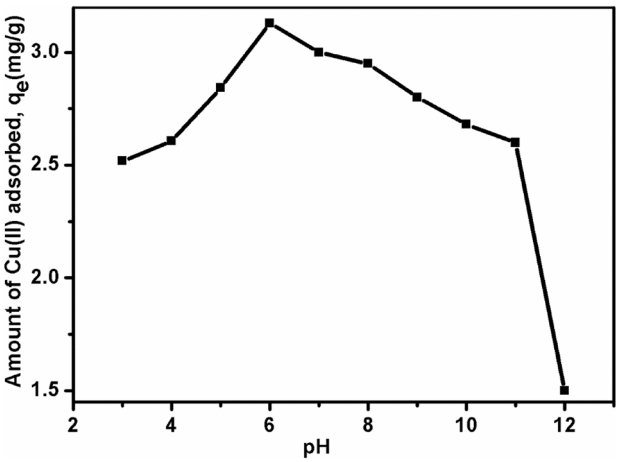

Fig. 8 Variation of the amount of copper adsorbed by synthesized AC with solution pH (optimized sample). [Reaction conditions: initial concentration = 30 ppm, adsorbent dosage = 0.2 g, temperature = 25 °C and rotation speed of shaker = 120 rpm]

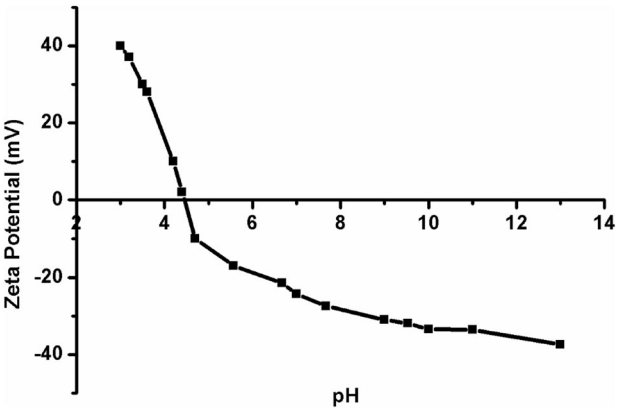

Fig. 9 Zeta potential of synthesized AC (optimized sample)

that the maximum uptake of Cu(II) (3.13 mg/g) was obtained at the pH 6. Increasing the pH from 6.5 to 12, a decrease in adsorption capacity was observed. A similar trend was observed by Tumin et al. (2008), where the adsorption capacity was increasing with increase in pH from 2 to 6, and a decrease was observed from pH 6 to 9. The minimum adsorption observed at pH 3 may be due to the fact that a higher concentration and mobility of H^+ ions present in the solution favoured the preferential adsorption of H^+ ions compared to Cu(II) ions (Ajmal et al. 2000; Li et al. 2007). Furthermore, it could be suggested that at lower pH value the AC surface is surrounded by hydronium ions thereby preventing the metal ions from approaching the binding sites of the adsorbent; in contrast, as the pH increases, more negatively charged surface becomes available thus facilitating greater copper removal (Wong et al. 2003; Tumin et al. 2008). However, at higher pH values (6.5–12), a decrease in the adsorption capacity is noticed due to copper precipitation which results in small quantities of Cu(II) ions, and large quantities of $Cu(OH)^+$ and $Cu(OH)_2$, such that these three species are adsorbed at the surface of the AC by ion-exchange mechanism or by hydrogen bonding. To understand the reasons for this, the zeta potentials of the synthesized optimized AC were investigated (Fig. 9). At the initial pH 3, the zeta potential of the synthesized AC (optimized sample) was 40 mV. When the initial pH of the solution was 4.3, the zeta potential was −12.18 mV. Thus, after a pH of 4.3, the synthesized activated carbon acts as a negative surface and attracts positively charged metal ions and the adsorption of Cu(II) was more effective. A similar decreased effect of adsorptive pH on adsorption capacity of other ACs caused by the formation of hydroxide complexes on the removal of copper was observed by other authors (Chen et al. 2011; Tumin et al. 2008). Therefore, in this study all subsequent adsorption experiments were carried out at pH 6.0 where the highest adsorption was attained.

Effect contact time

Contact time is a very important parameter in adsorption processes. It determines the equilibrium time of the adsorption process. The characteristics of activated carbon and its available adsorption sites affects the time needed to reach equilibrium. The adsorption was studied as a function contact time in the range 0–140 min using 30 ppm Cu(II) solution and at pH 6 for a 0.2 g of baobab fruit shell-derived AC. The results presented in Fig. 10 show that the adsorption capacity increased with increase in contact time up to 60 min. The results also show that large amounts of copper were removed in the first 60 min and equilibrium was attained between 60 and 80 min (95% adsorption of copper) and thereafter adsorption efficiency decreased significantly. The reason for this observation is that at the beginning of the adsorption process, all the adsorption sites on the surface of the synthesized AC were vacant and hence solute concentration gradient was relatively high. Subsequently after attaining equilibrium, the extent of copper(II) ion removal decreased with increase in contact time, which is dependent on the number of vacant sites on the surface of the synthesized AC. Apparently, the adsorption of most metal ions by activated carbon generally reaches equilibrium within 120 min (Mailler et al. 2016; Hasar 2004). Özçimen and Ersoy-Meriçboyu (2009) reported that the removal of copper from aqueous solution with a minimum contact time of 90 min for chestnut shell- and 120 min for grape seed-activated carbons. Therefore, based on these results, 75 min was taken as the equilibrium time for further experiments.

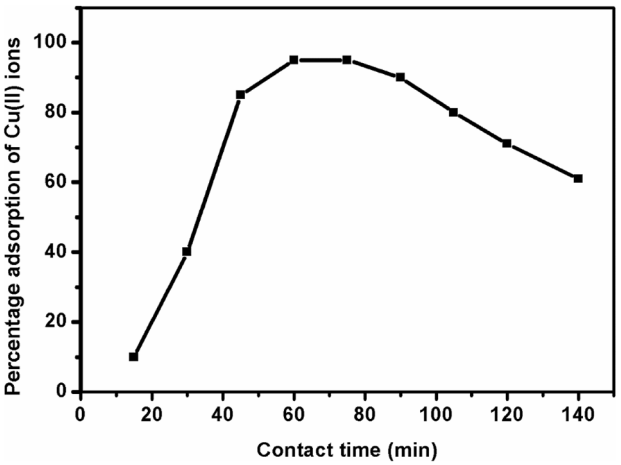

Fig. 10 Effect of contact time on copper ion adsorption onto synthesized AC (optimized sample). [Reaction conditions: pH = 6, initial concentration = 30 ppm, adsorbent dosage = 0.2 g, temperature = 25 °C and rotation speed of shaker = 120 rpm]

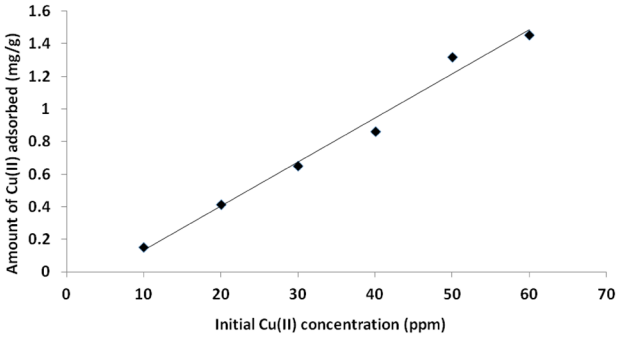

Fig. 11 Effect of initial copper concentration on copper ions adsorption onto synthesized AC (optimized sample). [Reaction conditions: pH = 6, adsorbent dosage = 0.2 g, temperature = 25 °C, rotation speed of shaker = 120 rpm and contact time = 75 min]

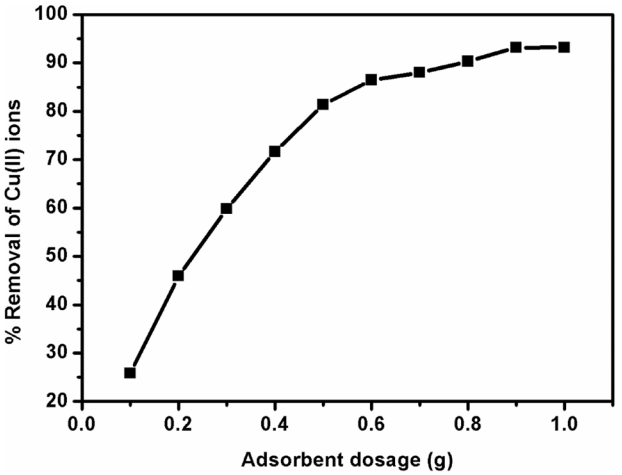

Fig. 12 Effect of adsorbent dosage on copper ions adsorption onto synthesized AC (optimized sample). [Reaction conditions: pH = 6, initial concentration = 30 ppm, temperature = 25 °C, rotation speed of shaker = 120 rpm and contact time = 75 min]

Effect of initial copper concentration

The initial concentration provides a good driving force to overcome all mass transfer resistance of Cu(II) ions between the aqueous solution and solid phase. Initial copper concentration on the adsorption process was investigated by varying initial metal ion concentration from 10 to 60 ppm and results are presented in Fig. 11. The results indicate that the actual amount of copper ions adsorbed (mg/g) increased with increase in the initial copper concentration. When the initial concentration was varied from 10 to 60 ppm, the adsorption capacity of synthesized AC derived from baobab fruit shell (optimized sample) increased from 0.14 to 1.5 mg/g. The increase in adsorption capacity of AC adsorbent with the increase in metal ion concentration is probably due to higher interaction between metal ions and adsorbent surface (Hanif et al. 2007). This is as a result of increase in the driving force of the concentration gradient as the initial copper concentration increases. It can be explained by the fact that a higher concentration of copper ions leads to an increase in the affinity of the metal ions towards the AC active sites.

Effect of adsorbent dosage

Adsorbent dosage is another important parameter because it determines the capacity of the adsorbent for a given copper concentration and also determines the sorbent–sorbate equilibrium of the system (Kilic et al. 2011). The effect of the adsorbent dosage on the adsorption of copper was carried out within the adsorbent dosage of 0.1–1.0 g of sample and results are shown in Fig. 12. It can be seen from Fig. 11 that the adsorption efficiency increases with increased in adsorbent dosage from 0.1 to 0.9 g up to a percentage removal of 93.17% and remained constant upon further increase of the AC dose. At a higher dosage, there is limited availability of adsorbing species for the relatively larger number of surface sites or surface area on the adsorbent. It is reasonable to say that at higher adsorbent dosage, there would be a greater availability of exchangeable sites or surface area (Tumin et al. 2008; Babel and Kurniawan 2004). It was noted that after an adsorbent dosage of 0.9 g, the adsorption efficiency did not increase significantly indicating the saturation of the adsorption sites. Similar observations have been reported by Mailler et al. (2016) for the adsorption of copper from aqueous solution onto green vegetable waste-derived carbon.

Effect of temperature

It is known that temperature has two major effects on the adsorption process. An increase in temperature increases the rate of diffusion of the adsorbate molecules across the external boundary layer and in the internal pores of the adsorbent particle because of a decrease in the viscosity of the solution. Changing the temperature will change the equilibrium capacity of the adsorbent for a particular adsorbate (Al-Qodah 2000). The effect of temperature on the percentage removal of copper by optimized AC was also investigated and is shown in Fig. 13. An increase in temperature from 25 to 50 °C increased the sorption of copper from 33 to 96%. This could be a result of the increased kinetic effect thus leading to increased mobility of the adsorbate molecules as temperature increases. The higher adsorption witnessed with increasing temperature indicates an endothermic and entropy-driven process.

Adsorption isotherms

Adsorption isotherms are mathematical models used to describe the distribution of the adsorbate species among the adsorbent and the liquid solution. This is usually based on assumptions related to the homogeneity/heterogeneity of adsorbents, possible interaction between the species and the type of coverage (Abdelkreem 2013). The results of adsorption isotherms are usually expressed as a plot of the concentration of chemical substance adsorbed (mg/g) versus the concentration remaining in solution (mg/L). These isotherms also provide insights into the possible course taken by the system under investigation, how efficient the adsorbent will adsorb and the economic viability of the adsorbent. In the present study, three isotherm models have been tested to analyse the equilibrium data of the synthesized activated carbon as adsorbent. Langmuir (Vunain et al. 2013), Freundlich (Lalhmunsiama et al. 2016) and Dubinin–Radushkevich models (Adekola et al. 2016) were employed to describe the sorption equilibrium data. The linear form of Langmuir isotherm is described by Eq. (7), and a plot of $\frac{C_e}{q_e}$ against c_e is shown in Fig. 14. The maximum adsorption capacity (q_m) and adsorption intensity (b) were determined from the slope and intercept, respectively, of the straight line.

$$\frac{C_e}{q_e} = \frac{1}{q_m b} + \frac{1}{q_m} c_e, \tag{7}$$

where q_e is the monolayer adsorption capacity of adsorbent (mg/g), C_e is the equilibrium concentration (mg/L), q_m is the maximum adsorption capacity that can be taken up per mass of adsorbent (mg/g), b (L/mg) is the Langmuir constant related to the sorption energy between the adsorbate and adsorbent.

To determine if the adsorption process was favourable or unfavourable, the dimensionless equilibrium constant (separation factor) R_L was calculated from the following equation:

$$R_L = \frac{1}{1 + q_m C_0}, \tag{8}$$

where C_0 is the highest initial metal concentration in solution (mg/L). When the value of $R_L > 1$, the adsorption process is unfavourable; linear, when $R_L = 1$; favourable when $0 < R_L < 1$; irreversible when $R_L = 0$ (Vunain et al. 2013; Garba and Rahim 2016). In our study, an R_L value of 0.0054 was obtained (which lies between 0 and 1), thus indicating a favourable adsorption of Cu(II) ions onto AC derived from baobab fruit shell. Generally, the separation

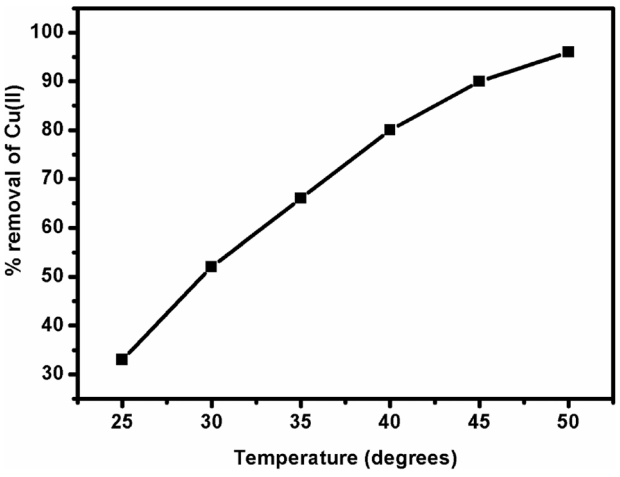

Fig. 13 Variation of percentage of copper adsorbed by synthesized AC with solution temperature (optimized sample). [Reaction conditions: pH = 6, initial concentration = 30 ppm, rotation speed of shaker = 120 rpm and contact time = 75 min]

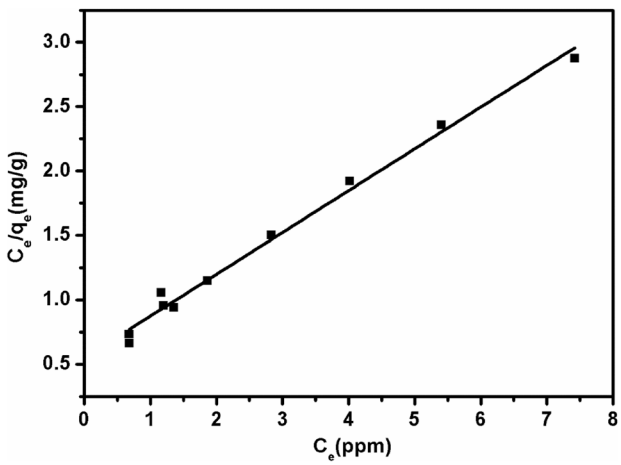

Fig. 14 Langmuir isotherm plot for the removal of Cu(II) onto synthesized AC (optimized sample)

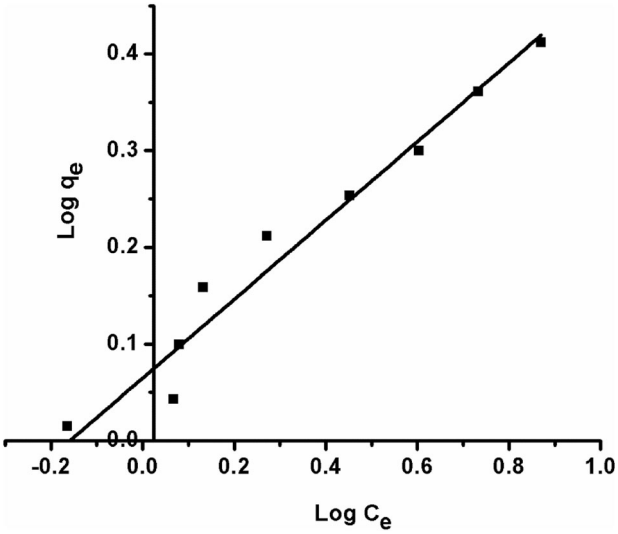

Fig. 15 Freundlich isotherm plot for removal of Cu(II) onto synthesized AC (optimized sample)

Table 4 Values of the used isotherm parameters at 25 °C

Isotherm model	Parameter	R^2
Langmuir	$q_m = 3.0833$	0.9987
	$b = 0.5889$	
	$R_L = 0.0054$	
Freundlich	$K_F = 1.16$	0.9634
	$n = 2.45$	
	$1/n = 0.41$	
Dubinin–Radushkevish	$q_m = 0.7429$	0.8216
	$\beta = 0.0072$	

factor between 0 and 1 gives rise to efficient adsorption performance.

The Freundlich model can be expressed as below:

$$\log q_e = \log K_F + \frac{1}{n} log C_e, \quad (9)$$

where q_e is the amount of copper adsorbed at equilibrium (mg/g), C_e is the equilibrium concentration of the adsorbate (mg/L); K_F and n are the Freundlich constants, which represent adsorption capacity and adsorption intensity, respectively. In this study, the values of K_F and n were obtained from the intercept and slope of a plot of $\log q_e$ versus $\log C_e$, respectively (Fig. 15).

Values of K_F and n are reported in Table 4. The values of n greater than one indicate that the adsorption is favourable under the conditions used in this study. The slope $1/n$ ranging between 0 and 1 is a measure of adsorption intensity or surface heterogeneity and becoming more heterogeneous as its value gets closer to zero. A value of $1/n$ below 1 indicates a normal Freundlich isotherm,

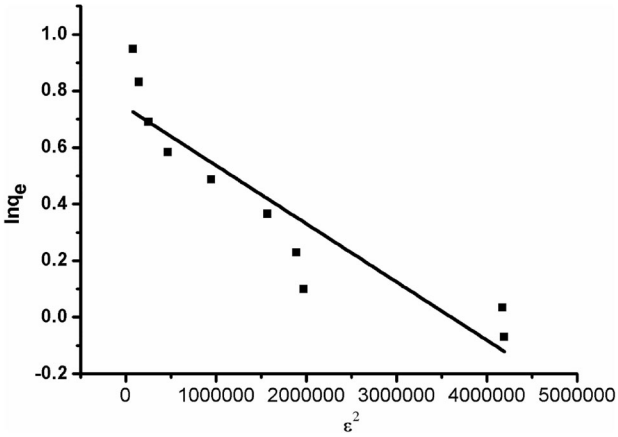

Fig. 16 D–R plot for removal of Cu(II) onto synthesized AC (optimized sample)

while $1/n$ above 1 indicates stronger sorption strength (Angin et al. 2013; Mahapatra et al. 2012; Angin 2014).

The Dubinin–Radushkevich (D–R) isotherm generally expressed as the following equation was also employed to fit the experimental data as illustrated in Fig. 16.

$$\ln q_e = \ln q_m - \beta\varepsilon^2, \quad (10)$$

where q_m represents the amount of copper adsorbed (mg/g) at equilibrium per unit weight of adsorbent, β is a constant related to the mean free energy of adsorption ($mmol^2/J^2$), and ε is the Polanyi potential which is related to the equilibrium concentration (C_e) measured in (J/mol), and expressed as:

$$\varepsilon = RT\left(1\frac{1}{C_e}\right), \quad (11)$$

where R is the universal gas constant (kJ/mol K) and T is the absolute temperature (K).

The constant, β, gives the mean free energy, E, of the sorption per molecule of the sorbate when it is transferred to the surface of the solid from infinity in the solution and can be calculated using the following expression (Vunain et al. 2013; González and Pliego-Cuervo 2014):

$$E = \frac{1}{\sqrt{2\beta}} \quad (12)$$

The isotherm constants q_m and β are obtained from the intercept and slope of a plot of $\ln q_e$ versus ε^2 and are found to be 0.7429 mg/g and 0.0072 mol^2/KJ^2, respectively.

The magnitude of E is very useful for estimating the type of adsorption process. The adsorption process can be described as chemical adsorption if the magnitude of E is between 8 and 16 kJ/mol and adsorption can be described as physical adsorption when the value is below 8 kJ/mol (due to weak van der Waals forces) (Köse et al. 2011; Vunain et al. 2013). In this study, the value of E was found

Table 5 Adsorption kinetic data for adsorption of Cu(II) by baobab fruit shell-derived activated carbon

Adsorption conditions	q_e(exp, mg/g)	Pseudo-first-order			Pseudo-second-order		
		k_1 (/min)	q_e (cal, mg/g)	R^2	k_2 (/min)	q_e (mg/g)	R^2
Concentration (ppm)							
10	1.7642	0.0113	0.9990	0.7423	0.1146	1.789	0.9984
20	2.7845	0.0259	0.1256	0.7812	0.1390	2.882	0.9997
30	3.0833	0.0413	1.9980	0.8698	0.2137	3.001	0.9990
40	5.8934	0.0439	2.340	0.8890	0.6892	5.804	0.9998
50	6.1290	0.0467	2.468i	0.8992	1.7807	6.689	0.9997
60	8.7101	0.1723	2.7045	0.8997	2.4456	8.790	0.9999
Temperature (°C)							
25	1.7148	0.0124	0.4562	0.7690	1.3489	1.7900	0.9910
30	1.7885	1.2670	1.2562	0.7856	2.5690	1.8802	0.9986
35	3.5633	1.7534	2.3478	0.8831	2.9823	3.6800	0.9993
40	4.8937	1.9802	2.8934	0.8884	3.0123	4.8890	0.9995
45	7.1670	2.3078	4.8912	0.8895	3.4534	7.2314	0.9997
50	9.9101	2.9078	5.1278	0.8961	4.5661	9.8567	0.9999

Conditions: adsorbent dosage = 0.2 g, pH = 6

to be 8.3333 kJ/mol. Therefore, the adsorption could be explained as chemical adsorption.

Comparing the R^2 values of the Langmuir, Freundlich and the Dubinin–Radushkevish isotherms, the Langmuir isotherm has a better fitting than the Freundlich and Dubinin–Radushkevish isotherms (Table 4). This was indicative of the formation of monolayer coverage of the Cu(II) adsorbate at the outer surface of the AC, and implies that the adsorption of Cu(II) ions is due to specific interactions of the metal ions with groups on the surface of the synthesized AC and no further adsorption occurs once a copper (II) molecule occupies a site.

Adsorption kinetics

Adsorption is mainly dependent on the ability of the synthesized AC to accumulate heavy metals from aqueous solutions by physicochemical pathways. Therefore, an evaluation of the mechanism such as mass transfer is necessary for kinetics studies (Mailler et al. 2016; Ricordel et al. 2001). Obviously, the mechanism of adsorption has to be validated by comparing the likely kinetic models. The adsorption kinetics of copper onto AC derived from baobab fruit shells were investigated using previously optimized conditions and data were tested using two well-known models: pseudo-first-order and pseudo-second-order models.

Pseudo-first-order kinetic model

The rate constant of adsorption is determined from the below pseudo-first-order equation (Rahim and Garba 2016).

$$\frac{dq_t}{dt} = k1(q_e - q_t), \tag{12}$$

where q_e and q_t (mg/g) are the amount of copper adsorbed at equilibrium and at time t (min), respectively. $k1$ is the rate constant for pseudo-first order (min^{-1}). When this equation is integrated under the boundary conditions $t = 0$ and $t = t$, $q = q_t$, the equation becomes:

$$\log(q_e - q_t) = \log q_e - \left(\frac{k1}{2.303}\right)t \tag{13}$$

A plot of $\log(q_e - q_t)$ versus t at various concentrations and temperatures resulted in linear graphs with negative slopes at all temperatures (figure not shown). The slope and intercepts of the plots were used to determine the first-order rate constant, $k1$, and the equilibrium adsorption capacity q_e, and values of these parameters are presented in Table 5. Although, the correlation coefficients (R^2) were high, comparison of the q_e calc. to the q_e exp. shows the values do not agree (see Table 5). Therefore, the adsorption of copper onto AC derived from baobab fruit shell does not follow pseudo-first-order kinetics.

The pseudo-second-order kinetics equation was also employed to describe the adsorption mechanism of copper in solution by containing all the steps during the adsorption process. The adsorption reaction of Cu(II) can be represented as the following equation:

$$2A + Cu^{2+} \rightarrow A_2Cu \tag{14}$$

Table 6 Comparison of sorption capacity of previous studies using agricultural wastes derived activated carbon for heavy metal removal

Adsorbent	Heavy metal	pH	q_e (mg/g)	Refs.
Activated carbon from palm oil mill effluent	Pb(II)	5–6	94.34	Abimbola et al. (2017)
	Zn(II)	5–6	68.49	
Activated carbon of palm oil empty fruit bunch	Cu(II)	4.4	0.84	Wahi et al. (2009)
Date pits activated carbon	Cu(II)	–	0.003	Bouchelta et al. (2012)
Cellulosic waste orange peel	Cu(II)	5.0	63	(Sami Guiza2017)
Activated carbon prepared from grape bagasse	Cu(II)	5.0	31.25	Demiral and Güngör (2016)
KOH-activated carbon derived from marine macroalga *Ulva lactuca*	Cu(II)	5.0	64.5–84.7	Ibrahim et al. (2016)
	Cd(II)		62.5–84.6	
	Cr(III)		60.9-82	
	Pb(II)		68.9–83.3	
Bio-char from oak bark	Pb(II)	–	0.516	Mohan et al. 2007)
	Cd(II)		0.213	
Baobab fruit shell-derived activated carbon	Cu(II)	5–6	3.0833	This study

The rate law for the reaction is expressed as below:

$$\frac{dq_t}{dt} = k_2(q_e - q_t)^2 \quad (15)$$

Thus, the pseudo-second-order kinetics in its linear forms as expressed by Ho and McKay (1999) is as follows:

$$\frac{t}{q_t} = \frac{1}{k_2 q_e^2} + \frac{1}{q_e}t \quad (16)$$

where k_2 [g/(mg/min)] and q_e (mg/g) are pseudo-second-order kinetic rate constant and adsorption capacity at equilibrium, respectively. If the pseudo-second-order equation is applicable, the plot of $\frac{t}{q_t}$ versus t would give a linear relationship with the values of k_2 and q_e obtained from the slope and intercept of the line, respectively (Figure not shown). Results are shown in Table 5 and the pseudo-second-order equation provides the best correlation coefficient with extremely high values (>0.99). The correlation coefficient of the pseudo-second-order model was close to 1, indicating that the rate-limiting step of the Cu(II) adsorption process was the chemical adsorption involving the valence force through electron sharing or exchange between the adsorbent (AC) and adsorbate Cu(II), since the formation of chemical bonds is one of the main factors influencing the pseudo-second-order kinetic adsorption. Furthermore, the calculated q_e values almost agreed with the experimental data in the case of the pseudo-second-order kinetics and, therefore, support the assumption that the chemical adsorption is rate limiting (Yao et al. 2016b; Ho and McKay 1999)

Validity of kinetic model

The applicability and fitting of isotherm equation to the kinetic data was compared by judging the correlation coefficient (R^2) values and the normalized standard deviation Δq_t (%) calculated from Eq. 17. The normalized standard deviation, Δq_t (%), was used to verify the kinetic model used to describe the kinetic adsorption. It is defined as:

$$\Delta q = 100\sqrt{\frac{\Sigma[(q_{exp} - q_{cal})/q_{exp}]^2}{n-1}}, \quad (17)$$

where n is the number of data points, q_{exp}, and q_{cal} (mg/g) are the experimental and calculated adsorption capacity values, respectively. Lower value of Δq_t indicates good fit between experimental and calculated.

Comparison of the adsorption capacities

Table 6 lists a comparative study of adsorption capacities for the prepared AC with those in the literature for removal of heavy metals from water and wastewater.

Comparison of treatment method, BET surface area and iodine number with those obtained in the literature

Table 7 shows comparison of data of treatment method, BET surface area and iodine number obtained in the present study with other literature reported values for different adsorbents.

Cost analysis

Adsorbent cost is a very important factor when it is used for industrial applications. The overall cost of an adsorbent such as activated carbon is determined by various factors such as its availability (natural, agricultural/domestic or industrial wastes or by-products or synthesized products),

Table 7 A comparison of the characteristics of the activated carbons with other literature reported values

Raw material	Treatment	BET surface area (m^2/g)	Iodine number (mg/g)	Refs.
Acorn shell	Physical activation, H_2O–CO_2	1779	1344	Sahin and Saka (2013)
Pistachio shell	Chemical activation, $ZnCl_2$	3256	–	Dolas et al. (2011)
Barley husks	Chemical activation, $ZnCl_2$	811.44	901.86	Loredo-Cancino et al. (2013)
Biomass (*Elaeagnus angustifolia seeds*)	Chemical activation, $ZnCl_2$	697	1009	Ceyhan et al. (2013)
Olive solid wastes	Chemical activation, H_3PO_4 and $ZnCl_2$	400/100 (H_3PO_4/$ZnCl_2$)	–	Zyoud et al. (2015)
Cotton stalks	Chemical activation with $ZnCl_2$, H_2SO_4 and physical activation using CO_2 and steam–CO_2 mixture	2053 ($ZnCl_2$ method)	–	Özdemir et al. (2011)
Pecan nuts (*Carya illinoinensis*)	Simple carbonization	691	–	Hernandez-Montoya et al. (2011)
Sweet and sour cherry kernels	Chemical, H_3PO_4	657.1	–	Pap et al. (2016)
Cashew nut shell	Chemical activation, $ZnCl_2$	456	–	Spagnoli et al. (2017)
Baobab fruit shell	Chemical activation, H_3PO_4	1089	1113	This study

the processing required and reuse (Chowdhury et al. 2011). Baobab fruit shell is readily obtained from the baobab tree largely available in abundance in the southern region of Africa (especially in Malawi) at no cost. In this work, the AC was chemically activated with phosphoric acid (H_3PO_4) as mentioned in the experimental section. However, it is expected that the activation process adds to the cost of preparing the adsorbent. An estimated cost per Kg of commercial activated carbon (Norit) from neighbouring South Africa (Sigma-Aldrich) is R 2,611.76 (equivalent to approximately 140,329.00 Malawi Kwachas). Comparing these figures, the cost of production of AC from baobab fruit shell is far more than 15 times cheaper than the commercially available activated carbon from South Africa.

Conclusions

The study has demonstrated the possibility of developing low-cost activated carbon from cheap and abundantly available Malawian baobab fruit shells and its potential as an effective adsorbent for the removal of copper ions from water and wastewater. The textural properties of the synthesized activated carbon are highly competitive to commercial activated carbon. Results showed that a pyrolysis temperature of 700 °C was the optimum pyrolysis condition to prepare carbon with maximum BET surface area, total pore volume and micropore volume of 1089 m^2/g, 0.4330 cm^3/g and 0.3764 cm^3/g, respectively. At this temperature, the material was faster to release volatile matters from the char to increase the specific surface area and the microporous volume. Thus, the carbon prepared at activation 700 °C showed excellent physicochemical properties than the other carbons (prepared at different temperatures) and was used as optimized sample in this study. The adsorption of copper onto baobab fruit shell-derived activated carbon (optimized sample) depends on factors such as pH, concentration of metal ions, contact time, adsorbent dosage, and temperature. The adsorption process revealed that the initial uptake was rapid and equilibrium was attained in about 75 min. The adsorption data fitted well into Langmuir isotherm model with a maximum adsorption capacity of 3.0833 mg/g. The separation factor, R_L, lies in between 0 and 1, indicating a favourable adsorption of copper from aqueous solution. Kinetic study shows that pseudo-second-order kinetic model fitted the adsorption process best. Cost analysis revealed that baobab fruit shell-derived activated carbon is cheaper than the commercially available activated carbon. Overall, the material (baobab tree) is not only economical but the fruit shell is an agricultural waste product. Thus, activated carbon prepared from baobab fruit shells would be useful for the economic treatment of wastewater containing some heavy metals ions such as copper metal ions because of its outstanding adsorption capacity, low-cost, non-toxic and biocompatibility. Based on the above findings, it is obvious that the baobab fruit shell-derived AC could be used as sorbent for the removal of other divalent metal ions such as Zn(II), Pb(II), Cd(II) and Ni(II), etc. from wastewater.

However, there are very important points that still need to be taken into account such as the development of preparation techniques, enhancement of the adsorption

extent by surface modification of the adsorbent, application for real industrial effluents, regeneration studies and treatment of multi-component mixtures.

Acknowledgements The authors would like to thank the Department of Chemistry, Chancellor College, University of Malawi for providing the research facilities and also the University Johannesburg, South Africa for the use of their SEM and XRD instruments for characterization. Many thanks to the Forest Research Institute of Malawi (FRIM) for the generous provision of data and statistics on baobab tree in Malawi.

References

Abdelkreem M (2013) Adsorption of phenol from industrial wastewater using olive mill waste. APCBEE Procedia 5:349–357

Abimbola GA, Zaman ZC, Adeniyi PA (2017) Equilibrium, kinetic, and thermodynamic studies of lead ion and zinc ion adsorption from aqueous solution onto activated carbon prepared from palm oil mill effluent. J Clean Prod 148:958–968

Adekola FA, Adegoke HI, Ajikanle RA (2016) Kinetic and equilibrium studies of Pb(II) and Cd(II) adsorption on African wild mango (*Irvingia gabonensis*) shell. Bull Chem Soc Ethiopia 30(2):185–198

Ajmal M, Rifaqat AKR, Rais A, Jameel A (2000) Adsorption studies on *Citrus reticulata* (fruit peel of orange): removal and recovery of Ni(II) from electroplating wastewater. J Hazard Mater 79(1–2):117–131

Akmil-bas C, Köseog E (2015) Preparation, structural evaluation and adsorptive properties of activated carbon from agricultural waste biomass. Adv Powder Technol 26:811–818

Ahmadpour A, Do DD (1996) The preparation of active carbons from coal by chemical and physical activation. Carbon 34:471–479

Al-Qodah Z (2000) Adsorption of dyes using shale oil ash. Water Res 34(17):4295–4303

Anchez AC (2011) The baobab tree in Malawi (University of Cambridge). Fruits 66(6):405–416

Angin D (2014) Utilization of activated carbon produced from fruit juice industry solid waste for the adsorption of Yellow 18 from aqueous solutions. Bioresour Technol 168:259–266

Angin D, Altintig E, Köse TE (2013) Influence of process parameters on the surface and chemical properties of activated carbon obtained from biochar by chemical activation. Bioresour Technol 148:542–549

Anisuzzaman SM, Colins GJ, Krishnaiah D, Bono A, Suali E, Abang S, Fai LM (2016) Removal of chlorinated phenol from aqueous media by guava seed (*Psidium guajava*) tailored activated carbon. Water Resour Industry 16:29–36

Babel S, Kurniawan TA (2004) Cr(VI) removal from synthetic wastewater using coconut shell charcoal and commercial activated carbon modified with oxidizing agents and/or chitosan. Chemosphere 54(7):951–967

Bohli T, Abdelmottaleb O, Nuria F, Isabel V (2015) Evaluation of an activated carbon from olive stones used as an adsorbent for heavy metal removal from aqueous phases. C R Chim 18:88–99

Bouchelta C, Mohamed SM, Marsa Z, Fatiha AC, Nassima R, Jean-Pierre B (2012) Effects of pyrolysis conditions on the porous structure development of date pits activated carbon. J Anal Appl Pyrolysis 94:215–222

Brito MJP, Cristiane V, Renata CFF, Keivison AM (2017) Activated carbons preparation from yellow mombin fruit stones for lipase immobilization. Fuel Process Technol 156:421–428

Ceyhan AA, Sahin Baytar O, Saka C (2013) Surface and porous characterization of activated carbon prepared from pyrolysis of biomass by two-stage procedure at low activation temperature and it's the adsorption of iodine. J Anal Appl Pyrolysis 104:378–383

Chen X, Guangcun C, Linggui C, Yingxu C, Johannes L, Murray BM, Anthony GH (2011) Adsorption of copper and zinc by biochars produced from pyrolysis of hardwood and corn straw in aqueous solution. Biores Technol 102(19):8877–8884

Chen YD, Huang MJ, Huang B, Chen XR (2012) Mesoporous activated carbon from inherently potassium-rich pokeweed by in situ self-activation and its use for phenol removal. J Anal Appl Pyrolysis 98:159–165

Chowdhury S, Mishra R, Saha P, Kushwaha P (2011) Adsorption thermodynamics, kinetics and isosteric heat of adsorption of malachite green onto chemically modified rice husk. Desalination 265(1–3):159–168

Daud WMAW, Houshamnd AH (2010) Textural characteristics, surface chemistry and oxidation of activated carbon. J Nat Gas Chem 19(3):267–279

Demiral H, Güngör C (2016) Adsorption of copper (II) from aqueous solutions on activated carbon prepared from grape bagasse. J Clean Prod 124:103–113

Deng H, Yang L, Tao G, Dai J (2009) Preparation and characterization of activated carbon from cotton stalk by microwave assisted chemical activation-application in methylene blue adsorption from aqueous solution. J Hazard Mater 166(2–3):1514–1521

Dolas H, Sahin O, Saka C, Demir H (2011) A new method on producing high surface area activated carbon: the effect of salt on the surface area and the pore size distribution of activated carbon prepared from pistachio shell. Chem Eng J 166:191–197

Ekpete OA, Horsfall MJNR (2011) Preparation and characterization of activated carbon derived from fluted pumpkin stem waste (*Telfairia occidentalis* Hook F). Res J Chem Sci 1(3):10–17

El-Demerdash FM, Abdullah AM, Ibrahim DA (2015) Removal of Trihalo methanes using activated carbon prepared from agricultural solid wastes. Hydrol Curr Res 6:1–6

Fadhil AB (2017) Evaluation of apricot (*Prunus armeniaca* L.) seed kernel as a potential feedstock for the production of liquid biofuels and activated carbons. Energy Convers Manag 133:307–317

Figueiredo J, Pereira MFR, Freitas MMA, Órfão JJM (1999) Modification of the surface chemistry of activated carbons. Carbon 37:1379–1389

Garba ZN, Abdul A (2016) Evaluation of optimal activated carbon from an para-chlorophenol and 2, 4-dichlorophenol. Process Saf Environ Prot 102:54–63

Garba ZN, Rahim AA (2016) Evaluation of optimal activated carbon from an agricultural waste for the removal of para-chlorophenol and 2,4-dichlorophenol. Process Saf Environ Prot 102:54–63

Ghouma I, Mejdi J, Sophie D, Lionel L, Camélia MG, Abdelmottaleb O (2015) Activated carbon prepared by physical activation of olive stones for the removal of NO_2 at ambient temperature. Inter Chem Eng Congress (ICEC) 2013: from fundamentals to applied Chem. Biochem 18(2):63–74

Gimba C, Musa I (2007) Preparation of activated carbon from agricultural waste: cyanide binding with activated carbon matrix from coconut shell. J Chem Nigeria 32:167–170

González PG, Pliego-Cuervo YB (2014) Adsorption of Cd(II), Hg(II) and Zn(II) from aqueous solution using mesoporous activated carbon produced from *Bambusa vulgaris* striata. Chem Eng Res Design 92(11):2715–2724

Guo Z, Jinlin F, Jian Z, Yan K, Hai L, Li J, Chenglu Z (2016) Sorption heavy metal ions by activated carbons with well-developed microporosity and amino groups derived from *Phragmites australis* by ammonium phosphates activation. J Taiwan Inst Chem Eng 58:290–296

Hanif MA, Nadeem R, Zafar MN, Akhtar K, Bhatti HN (2007) Kinetic studies for Ni(II) biosorption from industrial wastewater by *Cassia fistula* (Golden Shower) biomass. J Hazard Mater 145(3):501–505

Hasar H (2004) Adsorption of nickel(II) from aqueous solution onto activated carbon prepared from almond husk. J Hazard Mater 24(3):49–57

Hernández-Montoya V, Mendoza-Castillo DI, Bonilla-Petriciolet A, Montes-Moránb MA, Pérez-Cruzc MA (2011) Role of the pericarp of *Carya illinoinensis* as biosorbent and as precursor of activated carbon for the removal of lead and acid blue 25 in aqueous solutions. J Anal Appl Pyrolysis 92:143–151

Ho YS, McKay G (1999) Pseudo-second-order model for sorption processes. Process Biochem 34(5):451–465

Ibrahim WM, Hassan AF, Azab YA (2016) Biosorption of toxic heavy metals from aqueous solution by *Ulva lactuca* activated carbon. Egypt J Basic Appl Sci 3(3):241–249

Karnib M, Ahmad K, Hanafy H, Zakia O (2014) Heavy metals removal using activated carbon, silica and silica activated carbon composite. Energy Procedia 50:113–120

Kilic M, Apaydin-Varol E, Pütün AE (2011) Adsorptive removal of phenol from aqueous solutions on activated carbon prepared from tobacco residues: equilibrium, kinetics and thermodynamics. J Hazard Mater 189(1–2):397–403

Köse TE, Demiral H, Öztürk N (2011) Adsorption of boron from aqueous solutions using activated carbon prepared from olive bagasse. Des Water Treat 29(1–3):110–118

Köseoglu E, Akmil-Başar C (2015) Preparation, structural evaluation and adsorptive properties of activated carbon from agricultural waste biomass. Adv Powder Technol 26(3):811–818

Lalhmunsiama, Diwakar T, Seung-Mok L (2016) Surface-functionalized activated sericite for the simultaneous removal of cadmium and phenol from aqueous solutions: mechanistic insights. Chem Eng J 283:1414–1423

Li N, Ma X, Zha Q, Kim K, Chen Y, Song C (2011a) Maximizing the number of oxygen-containing functional groups on activated carbon by using ammonium persulfate and improving the temperature-programmed desorption characterization of carbon surface chemistry. Carbon 49(15):5002–5013

Li N, Almarri M, Ma XL, Zha QF (2011b) The role of surface oxygen-containing functional groups in liquid-phase adsorptive denitrogenation by activated carbon. New Carbon Mater 26(6):470–478

Li X, Yanru T, Zhexian X, Yinghui L, Fang L (2007) Study on the preparation of orange peel cellulose adsorbents and biosorption of Cd^{2+} from aqueous solution. Sep Purif Technol 55(1):69–75

Liou TH (2010) Development of mesoporous structure and high adsorption capacity of biomass-based activated carbon by phosphoric acid and zinc chloride activation. Chem Eng J 158:129–142

Lo SF, Wang SY, Tsai MJ, Lin LD (2012) Adsorption capacity and removal efficiency of heavy metal ions by Moso and Ma bamboo activated carbons. Chem Eng Res Design 90(9):1397–1406

Loredo-Cancino M, Soto-Regalado E, Cerino-Córdova FJ, García-Reyes RB, García-León AM, Garza-González MT (2013) Determining optimal conditions to produce activated carbon from barley husks using single or dual optimization. J Environ Manag 125:117–125

Lu X, Jianchun J, Kang S, Xinping X, Yiming H (2012) Surface modification, characterization and adsorptive properties of a coconut activated carbon. Appl Surf Sci 258(20):8247–8252

Lua AC, Yang T, Guo J (2004) Effects of pyrolysis conditions on the properties of activated carbons prepared from pistachio-nut shells. J Anal Appl Pyrolysis 72:279–287

Luo JJ, Jingjing L, Qiang N, Xiaobao Ch, Zhongye W, Jieru Z (2015) Preparation and characterization of benzoic acid-modified activated carbon for removal of gaseous mercury chloride. Fuel 160:440–445

Mahapatra K, Ramteke DS, Paliwal LJ (2012) Production of activated carbon from sludge of food processing industry under controlled pyrolysis and its application for methylene blue removal. J Anal Appl Pyrolysis 95:79–86

Mailler R, Gasperi J, Coquet Y, Deromea C, Buleté A, Vulliet E, Bressy A, Varrault G, Chebbod G, Rocher V (2016) Removal of emerging micropollutants from wastewater by activated carbon adsorption: experimental study of different activated carbons and factors influencing the adsorption of micropollutants in wastewater. J Environ Chem Eng 4:1102–1109

Mendoza-carrasco R, Mendoza-Carrasco R, Cuerda-Correa EM, Alexandre-Franco MF, Fernández-González C, Gómez-Serrano V (2016) Preparation of high-quality activated carbon from polyethyleneterephthalate (PET) bottle waste. Its use in the removal of pollutants in aqueous solution. J Environ Manag 181:522–535

Mohan D, Pittman CU Jr, Bricka M, Smith F, Yancey B, Mohammad J, Steele PH, Alexandre-Franco MF, Gómez-Serrano V, Gong H (2007) Sorption of arsenic, cadmium, and lead by chars produced from fast pyrolysis of wood and bark during bio-oil production. J Colloids Interf Sci 310:57–73

Moreno-Piraján JC, Giraldo L (2011) Activated carbon obtained by pyrolysis of potato peel for the removal of heavy metal copper (II) from aqueous solutions. J Anal Appl Pyrolysis 90(1):42–47

Nabil MM, Muhammad Abbas AZ, Zainul Akmar Z (2015) Preparation and characterization of activated carbon from pineapple waste biomass for dye removal. Inter Biodeterior Biodegrad 102:274–280

Nebagha KC, Ziat K, Lotfi R, Mohamed K, Mohamed S, Khadija A, Abderrahim El H, Said S (2015) Adsorptive removal of copper (II) from aqueous solutions using low cost Moroccan adsorbent. Part I: parameters influencing Cu (II) adsorption. J Mater Environ Sci 6(11):3022–3033

Nezamzadeh-ejhieh A, Kabiri-samani M (2013) Effective removal of Ni (II) from aqueous solutions by modification of nano particles of clinoptilolite with dimethylglyoxime. J Hazard Mater 260:339–349

Özçimen D, Ersoy-Meriçboyu A (2009) Removal of copper from aqueous solutions by adsorption onto chestnut shell and grapeseed activated carbons. J Hazard Mater 168(2–3):1118–1125

Özdemir M, Bolgaz T, Saka C, Sahin O (2011) Preparation and characterization of activated carbon from cotton stalks in a two-stage process. J Anal Appl Pyrolysis 92:171–175

Pap S, Radonic J, Trifunovic S, Adamovic D, Mihajlovic I, Vojinovic M, Miloradov MV, Sekulic MT (2016) Evaluation of the adsorption potential of eco-friendly activated carbon prepared from cherry kernels for the removal of Pb^{2+}, Cd^{2+} and Ni^{2+} from aqueous wastes. J Environ Manag 184:297–306

Qureshi K, Bhattiet I, Kazi RA, Khalique Ansari AQ (2008) Physical and chemical analysis of activated carbon prepared from sugarcane bagasse and use for sugar decolorisation. Inter J Chem Biomol Eng 1(3):145–149

Rahim AA, Garba ZN (2016) Efficient adsorption of 4-Chloroguiacol from aqueous solution using optimal activated carbon: equilibrium isotherms and kinetics modeling. J Assoc Arab Univ Basic Appl Sci 21:17–23

Ricordel S, Taha S, Cisse I, Dorange G (2001) Heavy metals removal by adsorption onto peanut husks carbon: characterization, kinetic study and modeling. Sep Purif Technol 24(3):389–401

Rivera-Utrilla J, Sánchez-Polo M, Gómez-Serrano V, Álvarezc PM, Alvim-Ferrazd MCM, Dias JM (2011) Activated carbon modifications to enhance its water treatment applications. An overview. J Hazard Mater 187(1–3):1–23

Rodriguez-Reinoso F, Molina-Sabio M (1992) Activated carbons from lignocellulosic materials by chemical and/or physical activation: an overview. Carbon 30:1111–1118

Saka C (2012) BET, TG-DTG, FT-IR, SEM, iodine number analysis and preparation of activated carbon from acorn shell by chemical activation with $ZnCl_2$. J Anal Appl Pyrolysis 95:21–24

Sahin O, Saka C (2013) Preparation and characterization of activated carbon from acorn shell by physical activation with H_2O–CO_2 in two-step pretreatment. Bioresour Technol 136:163–168

Guiza Sami (2017) Biosorption of heavy metal from aqueous solution using cellulosic waste orange peel. Ecol Eng 99:134–140

Scala F, Chirone R, Lancia A (2011) Elemental mercury vapor capture by powdered activated carbon in a fluidized bed reactor. Fuel 90(6):2077–2082

Sing KSW, Haul RAW, Pierotti RA (1985) Reporting physisorption data for gas/solid systems with special reference to the determination of surface area and porosity. Pure Appl Chem 57(4):603–619

Spagnoli AA, Giannakoudakis DA, Bashkova S (2017) Adsorption of methylene blue on cashew nut shell based carbons activated with zinc chloride: the role of surface and structural parameters. J Mol Liq 229:465–471

Tongpoothorn W, Sriuttha M, Homchan P, Chanthai S, Ruangviriyachai C (2011) Preparation of activated carbon derived from *Jatropha curcas* fruit shell by simple thermo-chemical activation and characterization of their physico-chemical properties. Chem Eng Res Design 89:335–340

Tounsadi H, Khalidi A, Machrouhi A, Farnane M, Elmoubarki R, Elhalil A, Sadiq M, Barka N (2016) Highly efficient activated carbon from *Glebionis coronaria* L. biomass: optimization of preparation conditions and heavy metals removal using experimental design approach. J Environ Chem Eng 4(4):4549–4564

Tran HN, You S-J, Chao H-P (2017) Fast and efficient adsorption of methylene green 5 on activated carbon prepared from new chemical activation method. J Environ Manag 188:322–336

Treviño-Cordero H, Juárez-Aguilar LG, Mendoza-Castillo DI, Hernández-Montoya V, Bonilla-Petriciolet A, Montes-Morán MA (2013) Synthesis and adsorption properties of activated carbons from biomass of *Prunus domestica* and *Jacaranda mimosifolia* for the removal of heavy metals and dyes from water. Ind Crops Prod 42(1):315–323

Trujillo-reyes J, Peralta-videa JR, Gardea-torresdey JL (2014) Supported and unsupported nanomaterials for water and soil remediation: are they a useful solution for worldwide pollution? J Hazard Mater 280:487–503

Tseng R-L (2007) Physical and chemical properties and adsorption type of activated carbon prepared from plum kernels by NaOH activation. J Hazard Mater 147(3):1020–1027

Tumin ND, Chuah AL, Zawani Z, Rashid SA (2008) Adsorption of copper from aqueous solution by *Elais Guineensis* kernel activated carbon. J Eng Sci Technol 3(2):180–189

Vunain E, Mishra AK, Krause RW (2013) Fabrication, characterization and application of polymer nanocomposites for arsenic(III) removal from water. J Inorg Organomet Polym Mater 23(2):293–305

Wahi R, Ngaini Z, Jok V (2009) Removal of mercury, lead and copper from aqueous solution by activated carbon of palm oil empty fruit bunch. World Appl Sci J 5:84–91

WHO (2004) Copper in drinking water: background document for development, WHO guidelines for drinking water quality, 2004

Wong KK, Lee CK, Low KS, Haron MJ (2003) Removal of Cu and Pb by tartaric acid modified rice husk from aqueous solutions. Chemosphere 50(1):23–28

Yang T, Lua AC (2003a) Characteristics of activated carbons prepared from pistachio-nut shells by physical activation. J Colloid Interf Sci 267:408–417

Yang T, Lua AC (2003b) Characteristics of activated carbons prepared from pistachio-nut shells by potassium hydroxide activation. Micropor Mesopor Mater 63:113–124

Yao S, Jiajun Z, Dekui S, Rui X, Sai G, Ming Z, Junyu L (2016a) Removal of Pb(II) from water by the activated carbon modified by nitric acid under microwave heating. J Colloid Interf Sci 463:118–127

Yao S, Zhang J, Shen D, Xiao R, Gu S, Zhao M, Liang J (2016b) Journal of colloid and interface science removal of Pb(II) from water by the activated carbon modified by nitric acid under microwave heating. J Colloid Interf Sci 463:118–127

Yuen FK, Hameed BH (2009) Recent developments in the preparation and regeneration of activated carbons by microwaves. Adv Colloid Interf Sci 149(1–2):19–27

Yusufu MI, Ariahu CC, Igbabul BD (2012) Production and characterization of activated carbon from selected local raw materials. AJPAC 6(9):123–131

Zhou JH, Sui ZJ, Jun Z, Ping L, De C, Dai YC, Yuan WK (2007) Characterization of surface oxygen complexes on carbon nanofibers by TPD, XPS and FT-IR. Carbon 45(4):785–796

Zhou Y, Zhang L, Cheng Z (2015) Removal of organic pollutants from aqueous solution using agricultural wastes: a review. J Mol Liq 212:739–762

Zyoud A, Nassar HNI, El-Hamouz A, Hilal HS (2015) Solid olive waste in environmental cleanup: enhanced nitrite ion removal by $ZnCl_2$-activated carbon. J Environ Manag 152:27–35